The structure of phenol-Ar$_n$ (n=1,2) clusters in their S_0 and S_1 states

Ivo Kalkman,[1] Christian Brand,[2] Thi-Bao Chau Vu,[2] W. Leo Meerts,[1] Yuriy N. Svartsov,[2] Otto Dopfer,[3] Xin Tong,[4] Klaus Müller-Dethlefs,[4] Stefan Grimme,[5] and Michael Schmitt[2,a)]

[1]*Molecular and Biophysics Group, Institute for Molecules and Materials, Radboud University Nijmegen, NL-6500 GL Nijmegen, The Netherlands*
[2]*Institut für Physikalische Chemie I, Heinrich-Heine-Universität, Universitätsstraße 26.43.02.43 D-40225 Düsseldorf, Germany*
[3]*Institut für Optik und Atomare Physik, Technische Universität Berlin, Hardenbergstraße 36, D-10623 Berlin, Germany*
[4]*The Photon Science Institute, The University of Manchester, Alan Turing Building, Manchester M13 9PL, United Kingdom*
[5]*Organisch-Chemisches Institut der Universität Münster, Corrensstrasse 40, D-48149 Münster, Germany*

(Received 2 March 2009; accepted 14 May 2009; published online 9 June 2009)

The structures of the van der Waals bonded complexes of phenol with one and two argon atoms have been determined using rotationally resolved electronic spectroscopy of the $S_1 \leftarrow S_0$ transition. The experimentally determined structural parameters were compared to the results of quantum chemical calculations that are capable of properly describing dispersive interactions in the clusters. It was found that both complexes have π-bound configurations, with the phenol-Ar$_2$ complex adopting a symmetric $(1|1)$ structure. The distances of the argon atoms to the aromatic plane in the electronic ground state of the n=1 and n=2 clusters are 353 and 355 pm, respectively. Resonance-enhanced multiphoton ionization spectroscopy was used to measure intermolecular vibrational frequencies in the S_1 state and Franck–Condon simulations were performed to confirm the structure of the phenol-Ar$_2$ cluster. These were found to be in excellent agreement with the $(1|1)$ configuration. [DOI: 10.1063/1.3149780]

I. INTRODUCTION

Intermolecular interactions of aromatic molecules are vital for chemical and biological recognition.[1] A detailed understanding of these interactions at the molecular level requires accurate knowledge of the intermolecular potential energy surface. Essential parameters of such a surface include the interaction energy and the geometry of the global minimum, as well as the occurrence of less stable local minima. The fruitful interplay of high-resolution spectroscopy of isolated clusters in molecular beams and high-level quantum chemical calculations provides the most direct access to these potential parameters.[2–9] Clusters of phenol with neutral ligands, denoted phenol-L_n, are attractive model systems to investigate the competition of two different fundamental types of intermolecular forces, namely hydrogen bonding to the acidic OH group (H-bond) and van der Waals (vdW) bonding (stacking) to the highly polarizable π electron system of the aromatic ring (π-bond, vdW bond). It turns out that the relative interaction strengths of both binding motifs strongly depend on the type of ligand (L), the degree of solvation (n), and the degree of electronic excitation or ionization. Hence, a plethora of spectroscopic and theoretical studies have been carried out on phenol-bearing clusters in order to determine the preference for stacking or hydrogen bonding interactions.

The present work reports high-resolution electronic spectra of phenol-Ar$_n$ clusters with n=1 and 2 in a molecular beam expansion, along with quantum chemical calculations. An analysis of vibrational frequencies from new resonance-enhanced multiphoton ionization (REMPI) spectra of the phenol-Ar$_n$ (n=1–2) clusters will corroborate the results. The analysis of the $S_1 \leftarrow S_0$ spectra obtained at the level of rotational resolution provides for the first time clear-cut information about the geometry and preferential binding motif of these prototype clusters, which are model systems for an acidic polar molecule interacting with a nonpolar solvent. Despite numerous spectroscopic studies on phenol-Ar$_n$ clusters reported in the past, the structural binding motif of this simple system has not been identified unambiguously for the neutral electronic states.

In the following, the present knowledge about phenol-Ar$_n$ will be briefly reviewed. In 1985, initial spectroscopic data about phenol-Ar$_n$ (n=0–2) came from one-color REMPI spectra of the $S_1 \leftarrow S_0$ transition and two-color photoionization efficiency (PIE) spectra of the cation ground state (D_0) recorded via the S_1 state origins by Gonohe *et al.*[10] On the basis of nearly additive shifts in the $S_1 \leftarrow S_0$ transition energies (-33 and -68 cm^{-1}) and ionization potentials (-152 and -297 cm^{-1}) upon complexation with one and two argon atoms, the authors concluded that both argon ligands are π-bonded to phenol on opposite sides of the aromatic ring, denoted $(1|0)$ and $(1|1)$ structure, respectively.[10] The intermolecular vibrational structures observed in the $S_1 \leftarrow S_0$ electronic spectra of phenol-Ar$_1$ (Refs. 11 and 12) and

a)Electronic mail: mschmitt@uni-duesseldorf.de.

phenol-Ar_2 (Ref. 13) have subsequently been assigned assuming π-bonded $(1|0)$ and $(1|1)$ structures, respectively.

Almost negligible complexation-induced frequency shifts of the O–H stretch (ν_{OH}) and other skeletal vibrations in the S_0 state of phenol-Ar_1 observed via stimulated Raman[14] and IR dip spectroscopy[15,16] have been indicative for a π-bonded $(1|0)$ geometry for the $n=1$ complex. In addition, high-level quantum chemical calculations of the potential energy surface in the S_0 state yield a π-bonded global minimum, and it is unclear at present whether the H-bonded structure is a shallow local minimum or a transition state.[17–20] Comparison of rotational constants derived from a rotational band contour fit of the S_1 origin spectrum with *ab initio* rotational constants obtained at the MP2/6-31G(d,p) level also support a π-bonded $(1|0)$ geometry for $n=1$.[21] Meerts *et al.*[6] presented the fully rotationally resolved electronic spectrum of the 7D-phenol-Ar_1 cluster, without a detailed structural analysis. The rotational constants of the S_0 state are close to those of the S_1 state, implying similar π-bonded geometries in both electronic states. Mass-analyzed threshold ionization (MATI) and zero-kinetic-energy (ZEKE) photoelectron spectroscopy have been employed to derive the binding energies of π-bonded phenol-Ar_1 in the D_0, S_1, and S_0 states as 535 ± 3, 397 ± 13 and 364 ± 13 cm^{-1}, respectively, and to measure and assign the intermolecular vibrational modes in the D_0 cation state.[22–25] The intermolecular frequencies are consistent with the π-bonded phenol-Ar_1 geometry. Similarly, the ν_{OH} frequency of phenol$^+$-Ar_1 derived from IR photodissociation of the cation dimer generated by REMPI is compatible only with a π-bonded isomer.[15,26]

Until recently, all spectroscopic studies indicated that phenol$^+$-Ar_1 has a π-bonded equilibrium structure in the S_0, S_1, and D_0 states and no signature of a H-bonded phenol$^+$-Ar_1 isomer had been detected. In 2000, however, the IR photodissociation spectrum of phenol$^+$-Ar_1 generated in an electron impact (EI) ion source clearly demonstrated that the H-bonded isomer is the global minimum on the potential energy surface of the cation cluster, with a characteristic ν_{OH} frequency strongly redshifted from isolated phenol$^+$ by H-bonding.[27–31] This result was confirmed by quantum chemical calculations, which predict the H-bonded isomer as global minimum in the D_0 state, whereas the π-bonded structure is only a local minimum.[20,28,32] The reason why the most stable H-bonded isomer of phenol$^+$-Ar_1 had completely escaped previous spectroscopic detection (MATI, PIE, ZEKE, REMPI-IR),[10,21,23–26] arises from the fact that the phenol$^+$-Ar cation in the D_0 state had been prepared by REMPI of the neutral π-bonded precursor, which is governed by the restrictions of minimal geometry changes imposed by the Franck–Condon (FC) principle. In contrast, the EI cluster ion source predominantly produces the most stable isomer of a given phenol$^+$-Ar_n cation cluster because the reaction sequence begins with EI ionization of the phenol monomer, which is followed by three body cluster aggregation reactions.[29,31] As the H-bond in phenol$^+$-Ar_1 is more stable than the π-bond, the energetically most favorable isomers of larger phenol$^+$-Ar_n clusters $(n>1)$ have one H-bonded ligand and $(n-1)$ π-bonded ones.[29]

The ionization-induced $\pi\rightarrow$H switch in the preferred phenol$\cdots$Ar binding motif has recently been probed by time-resolved IR spectroscopy of the phenol$^+$-Ar_2 complex prepared by REMPI.[33,34] These studies revealed that after ionization of π-bonded phenol-Ar_2, one Ar ligand isomerizes from the π-bonded site toward the H-bonded site on a time scale of several picoseconds. However, it was noted that for a full understanding of this dynamic process, one must know whether the neutral phenol-Ar_2 precursor complex has a symmetric $(1|1)$ structure with one Ar above and the other symmetrically below the aromatic plane or a $(2|0)$ structure with both Ar atoms at the same side of the aromatic ring. Unfortunately, no reliable calculations are available for the potential energy surface of phenol$^+$-Ar_2. Moreover, spectroscopic evidence for the geometric structure of neutral phenol-Ar_2 is scarce and not unambiguous as it relies on vibrationally resolved spectra only.[10,13,25,35] Recent hole-burning spectra of phenol-Ar_n with $n=1$ and 2 demonstrated that all spectral features observed in the $S_1\leftarrow S_0$ REMPI spectra indeed arise from single isomers in the molecular beam expansion, which have been assigned to π-bonded structures for both $n=1$ and $n=2$. The refined analysis of the intermolecular vibrational structure observed for phenol-Ar_2 was, however, compatible with both a $(1|1)$ and a $(2|0)$ structure.[35] The main purpose of the present work is to provide the definitive answer to the question of the geometry of the phenol-Ar_2 trimer.

II. METHODS

A. Experimental procedures

The experimental setup for rotationally resolved laser induced fluorescence spectroscopy is described in detail elsewhere.[36] Briefly, it consists of a ring dye laser (Coherent 899-21) operated with Rhodamine 110, pumped with 7 W of the frequency-doubled output of a diode pumped Yb:YAG (yttrium aluminum garnet) disk laser (ELS Versadisk). About 600–700 mW of the fundamental dye laser output is coupled into an external folded ring cavity (Spectra Physics) for second harmonic generation. The typical output power is 20 mW and is constant during each experiment. The molecular beam is formed by expanding phenol, heated to 365 K, and seeded in 600 mbars of argon, through a 230 μm hole into the vacuum. The molecular beam machine consists of three differentially pumped vacuum chambers that are connected by two skimmers (1 and 3 mm diameter, separated approximately 200 mm) in order to reduce the Doppler width to 25 MHz. The molecular beam is crossed at right angles with the laser beam in the third chamber, 360 mm downstream of the nozzle. The resulting fluorescence is collected perpendicular to the plane defined by the laser and the molecular beam by an imaging optics setup consisting of a concave mirror and two planoconvex lenses. The fluorescence is detected by a UV enhanced photomultiplier tube whose output is recorded by a PC based photon counter card. The relative frequency is determined with a quasiconfocal Fabry–Pérot interferometer. The absolute frequency is determined by recording the iodine absorption spectrum and comparison of the transitions with tabulated lines.[37]

The experimental apparatus for REMPI spectroscopy has been described in detail previously.[38] Phenol-Ar$_n$ clusters were produced in a skimmed supersonic expansion by passing argon gas over a heated phenol sample (330–350 K) in an internal sample holder located directly behind the valve. The pressure of argon gas can be varied up to 8 bars in order to optimize the production of phenol-Ar$_n$ clusters. The rotational temperature of the molecules is approximately 4 K after the expansion.[21] The molecular beam interacts with the counterpropagating, frequency-doubled output of two Nd:YAG pumped dye lasers (Radiant Dyes, Narrow Scan) using Coumarin 153 for excitation, while a mixture of sulforhodamine B and 4-dicyanomethylene-2-methyl-6-p-dimethylaminostyryl-4H-pyran (DCM) was used for the ionization laser to achieve a wide tuning range. The lasers were calibrated (± 0.02 cm^{-1}) with reference to simultaneously recorded iodine absorption spectra, corrected from air to vacuum.

Phenol was purchased from Riedel–de Haën and was used without further purification. 7D-phenol was produced by refluxing phenol with an excess of D_2O and subsequent removal of solvent.

B. Computational methods

1. Quantum chemical calculations

Quantum chemical calculations were performed with the TURBOMOLE (Ref. 39) and ORCA (Ref. 40) program packages. The Gaussian atomic orbital basis sets were taken from the TURBOMOLE library.[41,42] The economic triple-zeta Ahlrichs-type sets with different numbers of polarization functions (TZVP or TZVPP) as well as the triple and quadruple-zeta sets of Dunning[43] including diffuse basis functions (aug-cc-pVTZ and aug-cc-pVQZ) have been employed. Using these sets a detailed basis set dependence study has been performed for the structure of phenol-Ar$_2$. The equilibrium geometries of the electronic ground and the lowest excited singlet states were optimized at the level of the approximate coupled cluster singles and doubles model (CC2) employing the resolution-of-the-identity approximation.[44,45] The CC2 method represents the simplest reliable *ab initio* treatment of electron correlation consistent for both ground and excited states, which is necessary to describe noncovalently bound complexes. In addition, we also considered the currently most accurate density functional theory (DFT) approach for noncovalent interactions, namely, a double-hybrid functional including empirical dispersion corrections (B2PLYP-D).[46,47] This method explicitly includes nonlocal correlation effects and yields very accurate results close to those of CCSD(T) for the widely used S22 benchmark set of vdW complexes. Full geometry optimizations using analytical B2PLYP-D gradients[48] were performed for this method and only ground states were considered.

2. Franck–Condon simulations

The change in a molecular geometry on electronic excitation can be determined from the intensities of absorption or emission bands using the FC principle. According to the FC principle the relative intensity of a vibronic band depends on the overlap integral of the vibrational wave functions in both electronic states, which is determined by the relative shift of the two potential energy curves connected by the vibronic transition along the normal coordinates Q of both states and the vibrations involved,

$$\mathrm{FC} = \left| \int [\Psi'(Q')]^* \Psi''(Q'') dQ' \right|^2 = \langle v', \ldots, v'_N | v'', \ldots, v''_N \rangle^2, \quad (1)$$

where the $\Psi(Q)$ are the N-dimensional vibrational wave functions. The normal coordinates Q' of the excited state and Q'' of the ground state are related by the linear orthogonal transformation given by Duschinsky.[49]

The program FCFIT (Ref. 50) determines the structural changes on electronic excitation from the experimentally determined intensity pattern. Simultaneously, the changes in the rotational constants are used in the fit to assess the ge-

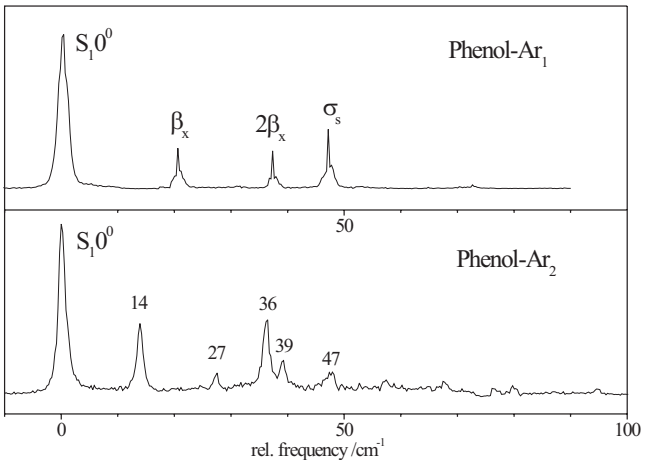

FIG. 1. Two-color $(1+1')S_1 \leftarrow S_0$ REMPI excitation spectra of phenol-Ar$_n$ ($n=1-2$). The spectra were recorded with the probe laser set to 32 210 cm^{-1}. Assignments of intermolecular modes are included for the $n=1$ complex. Frequencies are relative to the electronic origin of the $n=1$ cluster at 36 315.05 and of the $n=2$ cluster at 36 280.94 cm^{-1}.

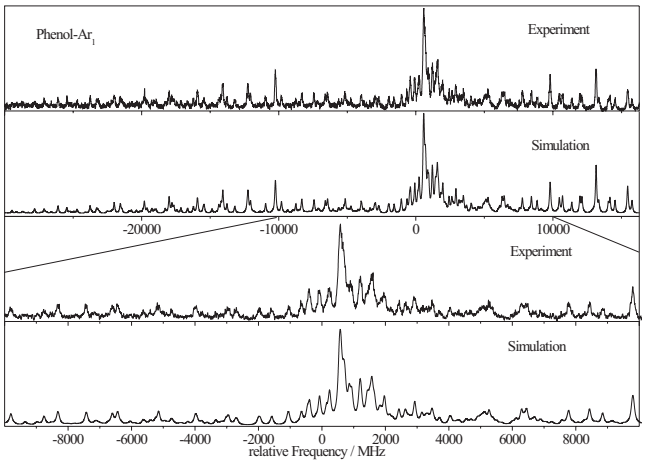

FIG. 2. Rotationally resolved spectrum of the electronic origin of the phenol-Ar$_1$ cluster at 36 315.05 cm^{-1} and simulation of the spectrum using the molecular parameters from the best ES fit, given in Table I. The lower two traces show an expanded view in the range from −10 000 to +10 000 MHz relative to the electronic origin.

TABLE I. Comparison of the molecular parameters from the fit to the rotationally resolved electronic spectrum of phenol-Ar_1 (Fig. 2) and 7D-phenol-Ar_1 (not shown), to the results of *ab initio* calculations. For the definition of the parameters, see text.

	Phenol-Ar_1			7D-phenol-Ar_1		
	Expt.	CC2[a]	B2PLYP-D[b]	Expt.	CC2[a]	B2PLYP-D[b]
A''/MHz	1818.7(5)	1804.00	1827.00	1780.1(5)	1760.85	1784.28
B''/MHz	1124.9(5)	1210.25	1200.86	1120.2(5)	1202.34	1191.87
C''/MHz	917.5(14)	973.25	971.28	905.5(7)	958.00	955.70
ϕ/(deg)	0[c]	0.36	⋯	0[c]	0.37	⋯
ΔA/MHz	−43.94(6)	−37.12	⋯	−43.44(3)	−34.61	⋯
ΔB/MHz	24.40(3)	31.66	⋯	25.19(2)	31.30	⋯
ΔC/MHz	23.35(2)	32.16	⋯	23.26(2)	31.44	⋯

[a]With the TZVP basis set.
[b]With the aug-cc-pVTZ basis set.
[c]Fixed to zero in the fit.

ometry change on excitation. The program was used to fit the intensities in the absorption spectrum using only the experimentally determined changes in the rotational constants. The necessary Hessians for ground and excited states were taken from the CC2/TZVP calculations.

3. Evolutionary strategies

The rotationally resolved electronic spectra were fit to an asymmetric rigid rotor Hamiltonian with the help of evolutionary strategies (ESs). Contrary to most previous applications of genetic algorithm techniques[51–53] in the evaluation of molecular parameters from rotationally resolved electronic spectra[6,54–56] a different ES with mutative step size control was used in the present work. Mutative step size control adapts the speed at which the parameter space is explored with each optimization step. It tends to work well for the adaptation of a global step size but tends to fail when it comes to the step size of each individual parameter due to several disruptive effects.[57] The derandomized algorithm DR2 used here[58] is aiming at the accumulation of information about the correlation or anticorrelation of past mutation vectors that connect trial solutions in order to tackle this problem. The high effectiveness of this approach for spectral analysis has been demonstrated recently.[59]

III. RESULTS AND DISCUSSION

A. REMPI spectra of phenol-Ar_{1-2}

REMPI spectra of the phenol-Ar_n ($n=1-2$) clusters are shown in Fig. 1. Spectroscopic results are in agreement with previous studies[23,25] but show considerable improvement in signal-to-noise ratio.

In the REMPI spectra of the phenol-Ar_1 cluster [Fig. 1(a)], the most intense feature, the S_1 band origin, appears at $36\,316.4 \pm 0.5$ cm^{-1}, in very good agreement with the previous value of $36\,316 \pm 0.5$ cm^{-1}.[23,25] The position of the origin transition represents a redshift of 33 cm^{-1} with respect to the S_1 origin of the phenol monomer at $36\,348.7$ cm^{-1}.[60] The spectrum also exhibits a number of vdW vibrational modes at 23, 42, and 53 cm^{-1} above the band origin. They have been previously assigned as the bending mode β_x, its overtone, $2\beta_x$, and the intermolecular stretch σ_s.[21]

The most prominent spectral feature in the phenol-Ar_2 spectrum [Fig. 1(b)] at $36\,282.1 \pm 0.5$ cm^{-1} is assigned to the $S_1 \leftarrow S_0$ origin. Relative to the phenol-Ar_1 band origin, this peak is redshifted by 34 cm^{-1}, suggesting that the argon atom solvates the phenol molecule at a similar binding site to that in phenol-Ar_1. In a previous study[35] several smaller visible features in the spectrum were assigned to a progression in an intermolecular bending vibration (β_x, $2\beta_x$, and $3\beta_x$ at 14, 27, and 39 cm^{-1}) and excitation of the intermolecular stretch (σ_s at 36 cm^{-1}). It was argued that this vibronic assignment is not unique and an asymmetric $(2|0)$ structure cannot be excluded for the phenol-Ar_2 cluster.[35]

B. Rotationally resolved electronic spectrum of phenol-Ar_1

The rotationally resolved electronic spectrum of the electronic origin of the phenol-Ar_1 cluster at $36\,315.05$ cm^{-1} is shown in Fig. 2. It is a nearly pure c-type spectrum which is dominated by a strong central Q-branch, shown in an expanded view in the lower trace of Fig. 2. Since no a- or b-type transitions could be incorporated unambiguously into the fit, the final fit was made to a pure c-type asymmetric rotor Hamiltonian. The same is true for the other high-resolution spectra discussed below.

Close agreement between the experimental spectrum and the simulation is obtained. The parameters deduced from this fit, listed in Table I, are the rotational constants in the S_0 state (A'', B'', C''), the change in rotational constants on electronic excitation $(\Delta(A,B,C))$, the frequency of the $S_1 \leftarrow S_0$ origin transition, and the direction of the transition dipole moment with respect to the system's main inertial a-axis (expressed in the angle ϕ).[56] The rotational temperature of the molecules in the molecular beam was described using a two temperature model[61,56] with $T_1=2.1$ K, $T_2=6.5$ K, and a relative weight factor of 0.01 for T_2. The Lorentzian width cannot be transformed into an excited state lifetime in this case, since the spectrum contains an unresolved torsional splitting due to the OH torsion and serves only to obtain

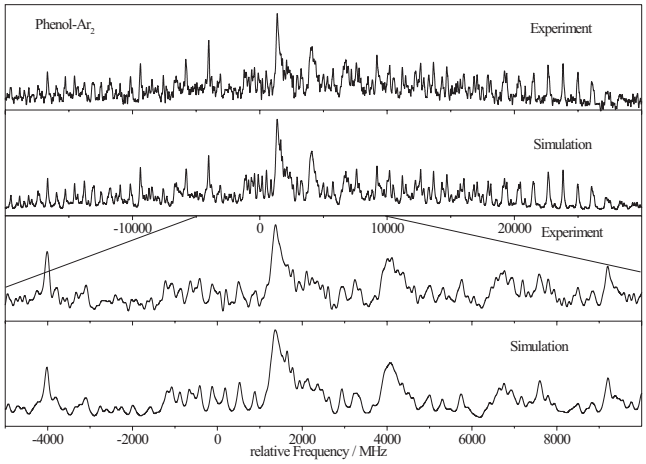

FIG. 3. Rotationally resolved spectrum of the electronic origin of phenol-Ar_2 at 36 280.94 cm^{-1} and simulation of the spectrum using the molecular parameters from the best ES fit, given in Table II. The lower two traces show an expanded view in the range of −9000 to +10 000 MHz relative to the electronic origin.

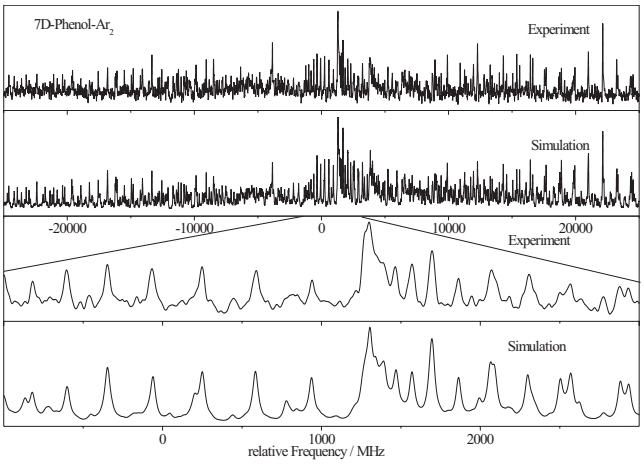

FIG. 4. Rotationally resolved spectrum of the electronic origin of 7D-phenol-Ar_2 at 36 278.62 cm^{-1} and simulation of the spectrum using the molecular parameters from the best ES fit (Table II). The lower two traces show an expanded view in the range of −1000–3000 MHz relative to the electronic origin.

good agreement between simulation and experiment.[62] The rotational constants of the ground state of phenol-Ar_1 determined from the high-resolution spectrum show significant deviations from those obtained from a contour fit to a low-resolution spectrum (with deviations of up to 4%),[21] demonstrating the limits of the latter technique for the extraction of quantitative structural information.

The second isotopologue which has been investigated is the 7D-phenol-Ar_1 cluster, which has its electronic origin at 36 312.74 cm^{-1} (spectrum not shown here). The linewidth of the rovibronic transitions in the deuterated cluster is considerably smaller than that of the undeuterated cluster, as is the case in the bare monomer.[60] A comparison of the molecular parameters obtained from the ES fits of the phenol-Ar_1 and 7D-phenol-Ar_1 spectra with the results of quantum chemical calculations is also given in Table I.

C. Rotationally resolved electronic spectrum of phenol-Ar_2

Figure 3 shows the rotationally resolved electronic spectrum of the phenol-Ar_2 origin at 36 280.94 cm^{-1}. As for the phenol-Ar_1 cluster, the spectrum is dominated by a strong Q-branch and can fully be simulated using selection rules for c-type bands. At 36 278.62 cm^{-1} the origin of its hydroxy deuterated isotopologue is found (Fig. 4). Also displayed are the simulations using the best fit parameters from Table II. Table II compares the molecular parameters obtained from ES fits of the phenol-Ar_2 and 7D-phenol-Ar_2 spectra with the results of quantum chemical calculations at different levels of theory and using different basis sets. For details about the calculations, cf. Sec. III E.

D. The structures of the phenol-$Ar_{1,2}$ clusters

The comparison of the experimental and calculated rotational constants of phenol-Ar_1 confirms that the cluster has a π-bound structure. Calculations also indicate the existence of a second stable structure, in which the argon atom is hydrogen bonded to the phenol OH group. However, this structure was not observed in the experiment. Both structures are depicted in Fig. 5. The structure of the phenol-Ar_2 cluster observed experimentally, however, has not been unequivocally determined yet. The most important clue concerning its

TABLE II. Comparison of the molecular parameters from the fit to the rotationally resolved electronic spectrum of phenol-Ar_2 and 7D-phenol-Ar_2 shown in Figs. 3 and 4, respectively, to the results of *ab initio* calculations of the (1|1) structure.

	Phenol-Ar_2			7D-phenol-Ar_2		
	Expt.	CC2[a]	B2PLYP-D[b]	Expt.	CC2[a]	B2PLYP-D[b]
A''/MHz	1777.6(5)	1774.10	1779.87	1726.4(5)	1724.23	1729.10
B''/MHz	462.5(3)	496.74	494.08	462.1(2)	496.41	493.77
C''/MHz	420.7(5)	449.69	447.42	417.8(2)	446.67	444.38
ϕ/(deg)	0[c]	0.35	⋯	0[c]	0.35	⋯
ΔA/MHz	−18.44(2)	−25.92	⋯	−15.45(2)	−22.76	⋯
ΔB/MHz	12.33(2)	19.23	⋯	12.31(2)	19.21	⋯
ΔC/MHz	13.23(2)	18.97	⋯	13.19(2)	18.85	⋯

[a]With the TZVP basis set.
[b]With the aug-cc-pVTZ basis set.
[c]Fixed to zero in the fit.

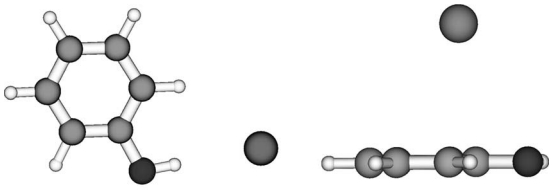

FIG. 5. Geometries of both considered phenol-Ar_1 isomers: The hydrogen bonded structure (left) and the vdW bonded structure (right).

structure is the rotationally resolved electronic spectrum of its S_1 origin. The rotational constants that can be expected for the different possible configurations (Fig. 6) are given in Table III. For the hydrogen bonded structure no changes in the rotational constants upon electronic excitation are given since no stable S_1 state minimum was found. Comparison with the experimental parameters from Table II provides unambiguous evidence for the $(1|1)$ structure of this cluster.

E. Structural parameters

The performance of different methods and basis sets for the prediction of the rotational constants and the distance of the argon atom(s) to the aromatic plane is compared in Table IV. Comparing the experimental with the calculated rotational constants, one has to bear in mind that the rotational constants from the calculations represent B_g^e $(g=a,b,c)$ values based on the r_e structure, while the experimental values are B_g^0 values based on the vibrationally averaged r_0 structure. We used Dunning's triple- and quadruple-ζ basis sets augmented with diffuse functions (aug-cc-pVTZ and aug-cc-pVQZ) as well as the Karlsruhe triple-ζ basis sets, augmented with single and double sets of polarization functions (TZVP and TZVPP) at the CC2 level. The argon atoms are located on the inertial a-axis, thus the motion of the argon atoms in the very shallow potentials parallel to the plane of phenol (the β_x and β_y vibrations, described in Sec. III F) will have a considerable effect on the B and C rotational constants. Especially, since the mean squared deviation due to zero-point vibration from the hypothetical equilibrium structure is positive, the experimental B and C rotational constants are expected to be smaller than the calculated ones. This is certainly the case here. A more thorough comparison of the effects of basis set size thus requires a correction of the calculated structure by zero-point vibrational effects in these weakly bound clusters. Calculations are on the way in order to obtain anharmonically corrected vibrationally averaged rotational constants on the respective level of theory. Since this procedure requires the computation of cubic and some of the quartic force constants at the respective level, this approach is extremely time-consuming and exceeds the scope of this article.

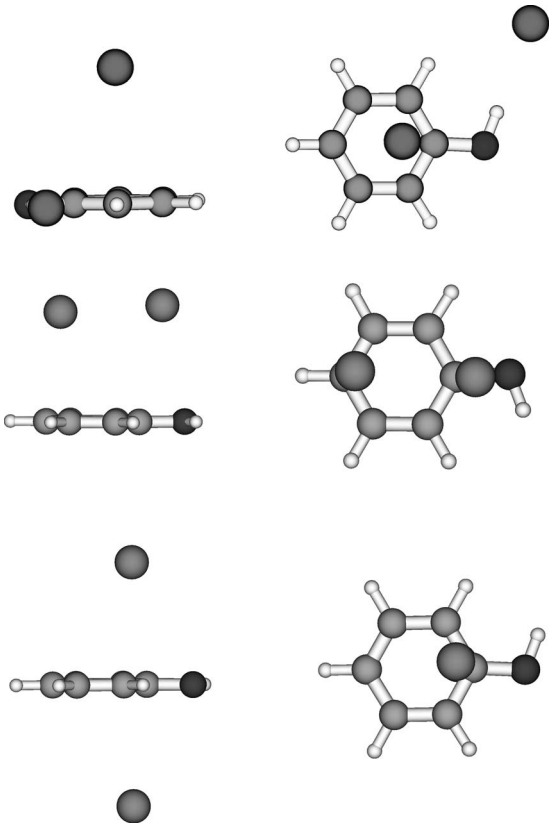

FIG. 6. Calculated geometries of various phenol-Ar_2 clusters (CC2/TZVP): the hydrogen bonded structure (top), the $(2|0)$ structure (middle), and the $(1|1)$ structure (bottom).

TABLE III. CC2/TZVP calculated rotational constants for several possible phenol-Ar_2 complexes (Fig. 6).

	VdW		
	$(1\|1)$	$(2\|0)$	Hydrogen bound
A''/MHz	1774.1	1095.4	1133.3
B''/MHz	496.7	651.7	443.3
C''/MHz	449.7	512.4	384.9
ΔA/MHz	−25.9	93.1	⋯
ΔB/MHz	19.2	−52.0	⋯
ΔC/MHz	19.0	−15.1	⋯

The intermolecular structures of the vdW bonded phenol-$Ar_{1,2}$ clusters were determined from the experimental rotational constants by means of a pseudo-Kraitchman fit[63] as described by Schmitt *et al.*[64] using the normal and hydroxy deuterated isotopologues. The use of pseudo-Kraitchman geometry parameters (r_s) has the advantage that the difference in the r_e structural parameters is smaller than for the rotational constants, which are based on r_0 values.[65,66]

For the $n=1$ cluster the perpendicular distance of the argon atom to the aromatic plane is given in Table IV and compared to the respective results from the B2PLYP-D/aug-cc-pVTZ and CC2/TZVP optimized structures. On electronic excitation, the argon distance decreases by more than 6 pm. This decrease can be traced back to the expected increase of dispersion energy for excited state complexes and to favorable orbital interactions that are repulsive in the ground state due to the Pauli exclusion principle.

For the $n=2$ cluster a slightly larger distance (about 2 pm) of the argon atom to the aromatic plane is observed for both the ground and the electronically excited state than for the $n=1$ cluster (cf. Table IV). For the *pseudo*-Kraitchman fit the distance of both argon atoms to the ring system was chosen to be the same. The experimentally determined dis-

TABLE IV. Calculated rotational constants and distance d of the argon atoms from the phenol plane obtained from a pseudo-Kraitchman fit in phenol-Ar_1 and phenol-Ar_2.

	CC2					
	TZVP	TZVPP	aug-cc-pVTZ	aug-cc-pVQZ	B2PLYP-D (aug-cc-pVTZ)	Expt.
				Phenol-Ar_1		
A''/MHz	1804.0	1813.1	1814.2	1815.8	1827.00	1818.7
B''/MHz	1210.3	1200.5	1225.9	1227.8	1200.86	1124.9
C''/MHz	973.3	969.5	986.8	988.9	971.28	917.5
$d(S_0)$/pm	340	341	337	338	341	352.6(9)
$d(S_1)$/pm	334	334	⋯	⋯	⋯	346.1(8)
				Phenol-Ar_2		
A''/MHz	1774.1	1755.6	1751.4	1757.5	1779.9	1777.6
B''/MHz	496.7	495.1	509.2	509.9	494.1	462.5
C''/MHz	449.7	447.2	458.5	459.2	447.4	420.7
$d(S_0)$/pm	344	345	336	336	342	354.5(2)
$d(S_1)$/pm	336	336	⋯	⋯	⋯	348.5(4)

tances in the $n=1$ and $n=2$ clusters agree reasonably well with the calculated parameters, with all experimental values being larger by 10–18 pm compared to the calculated values depending on the level of theory and basis set employed. A similar overestimation of binding energy and corresponding underestimation of intermolecular distances as known for MP2 (Ref. 67) can be expected with CC2 for the here considered phenol-Ar_n complexes. Thus, also the currently most accurate DFT approach for noncovalent interactions, a double-hybrid functional including empirical dispersion corrections[47] is included in Table IV and is compared to the CC2 values. It yields for both clusters better agreement than CC2 with the most appropriate basis set (aug-cc-pVQZ). The shorter distances of the calculations compared to the experiments have to be traced back to both overestimation of binding energy and the lack of inclusion of vibrational zero-point averaging in the calculations. Both typically contribute 5 pm in the intermolecular distances, yielding a very good agreement with the experimental value.

In order to understand why the distance of the argon atoms to the phenol ring is larger for the $n=2$ cluster, a decomposition of the total binding energy of the argon atoms to the phenol ring into its constituents [energy decomposition analysis (EDA), for details see, e.g., Ref. 68] is presented in Table V. Calculations were done at the B97-D/def2-TZVP EDA level of theory using the CC2/aug-cc-pVTZ optimized geometry. To enable this comparison the geometry used for the phenol-Ar_1 complex was that of the Phenol-Ar_2 complex with one of the argon atoms removed. The contribution per argon atom due to dispersion interaction is exactly equal for both $n=1$ and $n=2$ clusters due to the DFT-D approximation used in this analysis. The Pauli exchange repulsion is nearly equal due to the fixed geometries employed, and only the induction and electrostatic terms are notably different. While the electrostatic term tends to stabilize the $n=2$ cluster even more, the induction term overcompensates this effect. Half of the sum of electrostatic and induction interactions for the $n=2$ cluster is about 0.05 kcal/mol smaller than the sum of electrostatic and induction for the $n=1$ cluster. This small but significant decrease in binding energy for the phenol-Ar_2 complex is consistent with a longer phenol-argon distance. The most likely explanation for the smaller induction component is that the symmetry of the phenol-Ar_2 complex does not allow for the existence of an induced dipole moment perpendicular to the phenol plane.

Finally, we note that the total binding energy of 0.903 kcal/mol (316 cm^{-1}) for phenol-Ar_1 is consistent with the experimental value of 364 ± 13 cm^{-1},[23] demonstrating that this theoretical level accounts in a semiquantitative fashion for the intermolecular forces in this cluster.

F. Vibrational frequencies

Table VI compares the vibrational frequencies for the phenol-Ar_2 cluster obtained from its REMPI spectrum (Fig. 1) with the CC2 S_1-state vibrational frequencies for the $(1|1)$ cluster. The frequencies are somewhat overestimated, but on the whole the agreement is satisfactory. To test whether the assignments given in Table VI are reasonable a FC simulation was performed using the geometries and the Hessian

TABLE V. Decomposition of the different contributions to the binding energy (in kcal/mol) of argon atoms to the phenol ring in the electronic ground state at the DFT-B97-D/def2-TZVP level. The dispersion contribution is exactly additive (compare values in last column, first and last rows) in the DFT-D treatment used.

Complex	Total	Pauli	Electrostatic	Induction	Electrostatic+induction	Dispersion
Phenol-Ar_1	−0.903	3.632	−1.382	−0.675	−2.057	−2.478
Phenol-Ar_2	−1.684	7.273	−2.822	−1.178	−4.000	−4.956
$\frac{1}{2}$phenol-Ar_2	−0.849	3.636	−1.411	−0.589	−2.000	−2.478

TABLE VI. Phenol-Ar_2 intermolecular vibrational frequencies (in cm^{-1}) as determined from Fig. 1 compared with CC2/TZVP calculated S_1-state vibrational frequencies for the $(1|1)$ cluster.

Experiment	CC2	Assignment
14	15	β_x^1
20[a]	19	β_y^1
27	28[b]	β_x^2
⋯	26	λ_x^1
36	51	σ_s^1
39	42[b]	β_x^3
⋯	61	λ_y^1
⋯	68	σ_a^1
47	69[b]	$\sigma_s^1+\beta_x^1$

[a]From Ref. 35.
[b]Harmonic combination and overtone bands.

matrix from the CC2 calculations of both electronic states and the changes in the rotational constants given in Table II. From the rotational constants of the two isotopologues phenol-Ar_2 and 7D-phenol-Ar_2 the changes of six rotational constants upon excitation are obtained and can be used in the fit. With these six changes in the rotational constants, five modes have been used as basis for the geometry distortion upon excitation. These modes are the lowest five intermolecular modes from Table VI. The result displayed in Fig. 7 shows good agreement with experiment, confirming the assignments of Table VI. In order to facilitate the comparison of the experimental and FC fitted spectrum the theoretical frequencies have been set to the values of the experimental ones.

The vibrational assignments show that all peaks in the REMPI spectrum can be explained as progressions and combinations of just two modes, β_x and σ_s. For transitions from the ground state, these two modes are the only ones that are allowed in C_{2v} symmetry, which is a near-symmetry group for the $(1|1)$ cluster.[35] Under its proper symmetry group, C_s, β_y also becomes allowed, although its transition strength is expected to be low. Indeed, this mode has been detected at

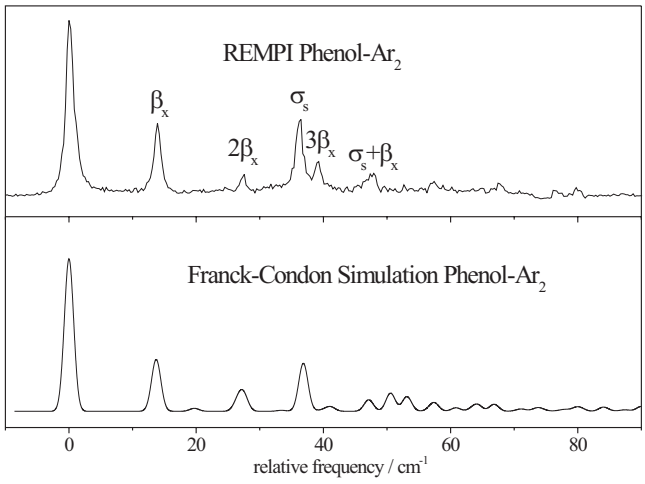

FIG. 7. FC simulation of the phenol-Ar_2 REMPI spectrum shown in Fig. 1(b). Frequencies are given with respect to the $S_1 \leftarrow S_0$ origin transition at 36 280.94 cm^{-1}. The corresponding peak assignments are given in Table VI.

20 cm^{-1} in the hole-burning spectrum of phenol-Ar_2 due to intensity enhancement arising from saturation effects of weak transitions. In contrast, the $(2|0)$ structure has C_1 symmetry and all six intermolecular vibrations are allowed in this isomer. The vibrational assignments of Table VI are therefore in agreement with the $(1|1)$ structure of the observed cluster.[35]

IV. CONCLUSIONS

The intermolecular structure of the phenol-Ar_n $(n=1,2)$ clusters has been investigated with high-resolution UV spectroscopy. From the rotational constants it could be deduced that in both clusters the argon atoms are vdW bonded to the phenol ring, with the $n=2$ cluster adopting a $(1|1)$ conformation where one argon atom is located on each side of the ring. Further evidence for these structures was extracted from REMPI spectra with the help of FC simulations. Quantum chemical calculations at the CC2 and B2PLYP-D levels of theory were performed to identify the most stable isomers, which are in full agreement with these assignments.

The distance between the argon atoms and the phenol ring was found to be slightly larger in the $n=2$ cluster than in the $n=1$ cluster. A decomposition of the cluster binding energy into individual contributions showed that this is due to a smaller inductive force between the ring and the argon atom in the $n=2$ cluster, arising from noncooperative three body induction interactions. Since the dominant inductive force arises from dipole-induced dipole interaction it was concluded that a small contribution to the induced dipole moment perpendicular to the phenol plane, which is forbidden by symmetry in the $n=2$ cluster, is most likely responsible for the smaller distance in the $n=1$ cluster.

ACKNOWLEDGMENTS

This work was supported by the Netherlands Organization for Scientific Research and the Deutsche Forschungsgemeinschaft in the framework of the NWO-DFG bilateral program (Grant No. SCHM1043/10). O.D. gratefully acknowledges financial support from the Deutsche Forschungsgemeinschaft (Grant No. DO729/2).

[1] E. A. Meyer, R. K. Castellano, and F. Diederich, Angew. Chem., Int. Ed. **42**, 1210 (2003).
[2] D. J. Nesbitt, Annu. Rev. Phys. Chem. **45**, 367 (1994).
[3] H. J. Neusser and K. Siglow, Chem. Rev. (Washington, D.C.) **100**, 3921 (2000).
[4] H. J. Neusser and H. Krause, Chem. Rev. (Washington, D.C.) **94**, 1829 (1994).
[5] E. J. Bieske and O. Dopfer, Chem. Rev. (Washington, D.C.) **100**, 3963 (2000).
[6] W. L. Meerts, M. Schmitt, and G. Groenenboom, Can. J. Chem. **82**, 804 (2004).
[7] M. Schmitt, C. Ratzer, and W. L. Meerts, J. Chem. Phys. **120**, 2752 (2004).
[8] T. M. Korter, J. Küpper, and D. W. Pratt, J. Chem. Phys. **111**, 3946 (1999).
[9] J. E. Braun, T. L. Grebner, and H. J. Neusser, J. Phys. Chem. A **102**, 3273 (1998).
[10] N. Gonohe, H. Abe, N. Mikami, and M. Ito, J. Phys. Chem. **89**, 3642 (1985).
[11] E. J. Bieske, M. W. Rainbird, I. M. Atkinson, and A. E. W. Knight, J. Chem. Phys. **91**, 752 (1989).
[12] M. Mons, J. L. Calve, F. Piuzzi, and I. Dimicoli, J. Chem. Phys. **92**, 2155

(1990).
[13] M. Schmidt, M. Mons, and J. L. Calve, Z. Phys. D: At., Mol. Clusters **17**, 153 (1990).
[14] G. V. Hartland, B. F. Henson, V. A. Venturo, and P. M. Felker, J. Phys. Chem. **96**, 1164 (1992).
[15] A. Fujii, M. Miyazaki, T. Ebata, and N. Mikami, J. Chem. Phys. **110**, 11125 (1999).
[16] T. Ebata, A. Iwasaki, and N. Mikami, J. Phys. Chem. A **104**, 7974 (2000).
[17] J. Makarewicz, J. Chem. Phys. **111**, 084310 (1999).
[18] F. Tran and T. A. Wesolowski, Int. J. Quantum Chem. **101**, 854 (2005).
[19] J. Cerny, X. Tong, P. Hobza, and K. Müller-Dethlefs, J. Chem. Phys. **128**, 114319 (2008).
[20] M. A. Vincent, I. H. Hillier, C. A. Morgado, N. A. Burton, and X. Shan, J. Chem. Phys. **128**, 044313 (2008).
[21] M. S. Ford, S. R. Haines, I. Pugliesi, C. E. H. Dessent, and K. Müller-Dethlefs, J. Electron Spectrosc. Relat. Phenom. **112**, 231 (2000).
[22] X. Zhang and J. L. Knee, Faraday Discuss. **97**, 299 (1994).
[23] C. E. H. Dessent, S. R. Haines, and K. Müller-Dethlefs, Chem. Phys. Lett. **315**, 103 (1999).
[24] C. E. H. Dessent and K. Müller-Dethlefs, Chem. Rev. (Washington, D.C.) **100**, 3999 (2000).
[25] S. R. Haines, C. E. H. Dessent, and K. Müller-Dethlefs, J. Electron Spectrosc. Relat. Phenom. **108**, 1 (2000).
[26] A. Fujii, T. Sawamura, S. Tanabe, T. Ebata, and N. Mikami, Chem. Phys. Lett. **225**, 104 (1994).
[27] N. Solca and O. Dopfer, Chem. Phys. Lett. **325**, 354 (2000).
[28] N. Solca and O. Dopfer, J. Mol. Struct. **563–564**, 241 (2001).
[29] N. Solca and O. Dopfer, J. Phys. Chem. A **105**, 5637 (2001).
[30] N. Solca and O. Dopfer, Chem. Phys. Lett. **369**, 68 (2003).
[31] O. Dopfer, Z. Phys. Chem. **219**, 125 (2005).
[32] J. Cerny, X. Tong, P. Hobza, and K. Müller-Dethlefs, Phys. Chem. Chem. Phys. **10**, 2780 (2008).
[33] S. Ishiuchi, M. Sakai, Y. Tsuchida, A. Takeda, Y. Kawashima, M. Fujii, O. Dopfer, and K. Müller-Dethlefs, Angew. Chem., Int. Ed. **44**, 6149 (2005).
[34] S. Ishiuchi, M. Sakai, Y. Tsuchida, A. Takeda, Y. Kawashima, O. Dopfer, K. Müller-Dethlefs, and M. Fujii, J. Chem. Phys. **127**, 114307 (2007).
[35] S. Ishiuchi, Y. Tsuchida, O. Dopfer, K. Müller-Dethlefs, and M. Fujii, J. Phys. Chem. A **111**, 7569 (2007).
[36] M. Schmitt, J. Küpper, D. Spangenberg, and A. Westphal, Chem. Phys. **254**, 349 (2000).
[37] S. Gerstenkorn and P. Luc, *Atlas du Spectre D'Absorption de la Molécule D'iode*14 800–20 000 cm^{-1} (CNRS, Paris, 1986).
[38] S. R. Haines, W. D. Geppert, D. M. Chapman, M. J. Watkins, C. E. H. Dessent, M. C. R. Cockett, and K. Müller-Dethlefs, J. Chem. Phys. **109**, 9244 (1998).
[39] R. Ahlrichs, M. Bär, and H.-P. Baron, TURBOMOLE (version 5.7), Universität Karlsruhe, Germany, 2002.
[40] F. Neese, ORCA, an *ab initio*, density functional and semiempirical program package, University of Bonn, Germany, 2007.
[41] R. Ahlrichs, M. Bär, M. Häser, H. Horn, and C. Kölmel, Chem. Phys. Lett. **162**, 165 (1989).
[42] A. Schäfer, C. Huber, and R. Ahlrichs, J. Chem. Phys. **100**, 5829 (1994).
[43] J. T. H. Dunning, J. Chem. Phys. **90**, 1007 (1989).
[44] C. Hättig and A. Köhn, J. Chem. Phys. **117**, 6939 (2002).
[45] C. Hättig, J. Chem. Phys. **118**, 7751 (2003).
[46] S. Grimme, J. Chem. Phys. **124**, 034108 (2006).
[47] T. Schwabe and S. Grimme, Phys. Chem. Chem. Phys. **9**, 3397 (2007).
[48] F. Neese, T. Schwabe, and S. Grimme, J. Chem. Phys. **126**, 124115 (2007).
[49] F. Duschinsky, Acta Physicochim. URSS **7**, 551 (1937).
[50] D. Spangenberg, P. Imhof, and K. Kleinermanns, Phys. Chem. Chem. Phys. **5**, 2505 (2003).
[51] J. H. Holland, *Adaption in Natural and Artificial Systems* (The University of Michigan Press, Ann-Arbor, MI, 1975).
[52] D. E. Goldberg, *Genetic Algorithms in Search, Optimisation and Machine Learning* (Addison-Wesley, Reading, MA, 1989).
[53] I. Rechenberg, *Evolutionsstrategie: Optimierung Technischer Systeme Nach Prinzipien der biologischen Evolution* (Frommann-Holzboog, Stuttgart, 1973).
[54] J. A. Hageman, R. Wehrens, R. de Gelder, W. L. Meerts, and L. M. C. Buydens, J. Chem. Phys. **113**, 7955 (2000).
[55] W. L. Meerts and M. Schmitt, Phys. Scr. **73**, C47 (2006).
[56] W. L. Meerts and M. Schmitt, Int. Rev. Phys. Chem. **25**, 353 (2006).
[57] N. Hansen and A. Ostenmeier, Evol. Comput. **9**, 159 (2001).
[58] A. Ostenmeier, A. Gawelcyk, and N. Hansen, *Step-Size Adaptation Based on Non-Local Use of Selection Information*, Parallel Problem Solving From Nature, Vol. 3 (Springer, Berlin/Heidelberg, 1994).
[59] I. Kalkman, C. Vu, M. Schmitt, and W. L. Meerts, ChemPhysChem **9**, 1788 (2008).
[60] C. Ratzer, J. Küpper, D. Spangenberg, and M. Schmitt, Chem. Phys. **283**, 153 (2002).
[61] Y. R. Wu and D. H. Levy, J. Chem. Phys. **91**, 5278 (1989).
[62] G. Berden, W. L. Meerts, M. Schmitt, and K. Kleinermanns, J. Chem. Phys. **104**, 972 (1996).
[63] P. Nösberger, A. Bauder, and H. H. Günthard, Chem. Phys. **1**, 418 (1973).
[64] M. Schmitt, D. Krügler, M. Böhm, C. Ratzer, V. Bednarska, I. Kalkman, and W. L. Meerts, Phys. Chem. Chem. Phys. **8**, 228 (2006).
[65] C. Costain, J. Chem. Phys. **29**, 864 (1958).
[66] J. K. G. Watson, J. Mol. Spectrosc. **48**, 479 (1973).
[67] T. B. W. Klopper, H. P. Lüthi, and A. Bauder, J. Chem. Phys. **101**, 9747 (1994).
[68] S. Grimme, J. Antony, T. Schwabe, and C. Mück-Lichtenfeld, Org. Biomol. Chem. **5**, 741 (2007).